# Coulomb energies in alloys

J. S. Faulkner
*Alloy Research Center and Department of Physics, Florida Atlantic University, Boca Raton, Florida 33431*

Yang Wang and G. M. Stocks
*Metals and Ceramics Division, Oak Ridge National Laboratory, Oak Ridge, Tennessee 37830*

(Received 25 March 1996; revised manuscript received 2 December 1996)

With the help of order-$N$ calculations on realistic models of random substitutional alloys, we have studied the concentration, structure, and composition dependence of the part of the total energy that is stored in the interatomic Coulomb interaction. An observation about the relation between the self-consistent charges associated with a site and the long-range electrostatic potential at the site is used in the analysis. [S0163-1829(97)01512-9]

## I. INTRODUCTION

Recently, there have been a number of theoretical studies of the part of the total energy of disordered alloys that is stored in the interatomic Coulomb energy.[1–9] We have calculated the electronic states of realistic models of disordered alloys within the local-density approximation[10] (LDA) using an order-$N$ method that is particularly well-adapted for calculations on transition metals, the locally self-consistent multiple-scattering method.[11] An analysis of the results of these calculations makes it possible for us to comment upon the concentration, structure, and composition dependence of the Coulomb energies of alloys. An analysis of earlier calculations led to the discovery of a relation between the self-consistent charge associated with a site and the long-range electrostatic potential at the site, which we call the $qV$ relation.[12] The $qV$ relation is used in the present study.

Most of the calculations are on the copper-zinc alloy system, which was chosen for several reasons. First, it is the classic example of a Hume-Rothery alloy,[13] and has been discussed extensively in the materials science literature. Since the constituents are both transition metals, experience from ordinary band-theory calculations leads us to expect that the muffin-tin approximation that we use will not introduce significant errors. Finally, there is no experimental or theoretical reason to believe that the size difference between copper and zinc would cause the rms deviation of the atomic positions from the sites of the ideal lattice to be significant. We also include some calculations on copper-palladium alloys for comparison.

In the following section we write out the LDA equations for the total energy in a form that is useful for the following discussion, and comment on possible sources of error. In Sec. III, we explain briefly the order-$N$ method, and show the results of our calculations on the total Coulomb energies in fcc and bcc alloys as a function of concentration. In Sec. IV, we discuss a number of theoretical questions, such as the convergence and reliability of the calculations and the meaning of the parameters that have been introduced. We also comment on the extrapolation of our results to obtain the properties of ideal disordered alloys. In Sec. V, we compare the predictions of theories proposed in the literature with the results of our calculations. In the last section we discuss our conclusions in the light of the preceding development and indicate future applications.

## II. BACKGROUND

### A. The Coulomb energy

The purpose of this section is to specify unambiguously the part of the total energy that we consider to be stored in the interatomic Coulomb interaction in the calculations to follow. The following equations highlight the fact that the Coulomb energy, the Coulomb potential at a site, and the charge associated with a site take on a particularly simple and unambiguous form when the muffin-tin approximation is used for the charge density. This result is not new, but it is not generally appreciated by those who have not carried out a detailed calculation of these quantities.

According to the density-functional theory[14] DFT, the total energy of a system of electrons and nuclei is a functional of the electron density $\rho(\mathbf{r})$. It is normally written in the form

$$E[\rho]=T[\rho]+E_H[\rho]+E_{\mathrm{xc}}[\rho], \tag{1}$$

where $T[\rho]$ is the kinetic-energy functional, $E_{\mathrm{xc}}[\rho]$ is the exchange-correlation energy functional, and

$$E_H[\rho]=\int \rho[\tfrac{1}{2}\phi+V_N]d\mathbf{r}+V_{NN} \tag{2}$$

is the Hartree energy functional that contains all the contributions from the Coulomb interactions between the particles.

In this paper, calculations will be carried out on systems that contain an infinite number of atoms. A cell containing $N$ atoms in any desired arrangement is constructed, and then it is periodically reproduced to fill all space. At the present time, $N$ can be as large as 1024. The charge density is written as a sum of nonoverlapping functions,

$$\rho(\mathbf{r})=\sum_{i=1}^{N}\sum_{p=1}^{N_c}\rho^i(\mathbf{r}-\mathbf{a}_i-\mathbf{R}_p), \tag{3}$$

where the positions of nuclei within the cells are given by the vectors $\mathbf{a}_i$, and the positions of the cells are determined by

 

the vectors $\mathbf{R}_p$. From the definition of the model, the charge $\rho^i(\mathbf{r}-\mathbf{a}_i-\mathbf{R}_p)$ is the same for all vectors $\mathbf{R}_p$, and the number of cells, $N_c$, will be allowed to increase without bound. The process for writing $\rho(\mathbf{r})$ in this way starts with the construction of polyhedral atomic volumes $\Omega_i$ centered at each of the atomic positions $\mathbf{a}_i+\mathbf{R}_p$ by passing planes perpendicular to lines connecting the atom with its neighbors. If the atomic positions form a regular lattice, these atomic volumes would have the same shape as the Wigner-Seitz cells for that lattice. The functions that appear in the sum in Eq. (3) are obtained by defining $\rho^i(\mathbf{r}-\mathbf{a}_i-\mathbf{R}_p)$ to be equal to $\rho(\mathbf{r})$ when $\mathbf{r}$ is within $\Omega_i$, and it is zero when $\mathbf{r}$ is outside of $\Omega_i$.

The functions that appear in the Hartree energy in Eq. (2), in addition to $\rho(\mathbf{r})$, are the Coulomb potential due to the electrons

$$\phi(\mathbf{r})=2\int \frac{\rho(\mathbf{r}')}{|\mathbf{r}-\mathbf{r}'|}\,d\mathbf{r}', \tag{4}$$

the potential due to the nuclei

$$V_N(\mathbf{r})=-\sum_{i=1}^{N}\sum_{p=1}^{N_c}\frac{2Z_i}{|\mathbf{r}-\mathbf{a}_i-\mathbf{R}_p|}, \tag{5}$$

and the interaction energy of the bare nuclei

$$V_{NN}=-\sum_{i,j=1}^{N}\sum_{p=1}^{N_c}{}'\frac{Z_iZ_j}{|\mathbf{a}_{ij}+\mathbf{R}_p|}, \tag{6}$$

with $\mathbf{a}_{ij}=\mathbf{a}_i-\mathbf{a}_j$. The prime on the summation sign indicates that the sum does not include the terms for which the denominator is zero. The factor 2 appears because dimensionless atomic units in which the energy is measured in Rydbergs, distances in Bohr radii, and the charge in electronic charges are used. Inserting these functions into the equation for the Hartree energy and making use of the invariance of the system under translation by a cell lattice vector $\mathbf{R}_p$ leads to

$$E_H[\rho]=N_c\left(\sum_{i=1}^{N}U_C^i[\rho^i]+U_C\right), \tag{7}$$

where $U_C^i[\rho^i]$ is the intra-atomic Coulomb energy for the atomic volume $\Omega_i$,

$$U_C^i[\rho^i]=\int_{\Omega_i}\rho^i(\mathbf{r})[\tfrac{1}{2}\phi^i(\mathbf{r})+V_N^i(\mathbf{r})]d\mathbf{r}, \tag{8}$$

and $U_C$ is the interatomic Coulomb energy

$$\begin{aligned}U_C=&\sum_{i,j=1}^{N}\sum_{p=1}^{N_c}{}'\int_{\Omega_i}\int_{\Omega_j}\frac{\rho^i(\mathbf{r})\rho^j(\mathbf{r}')}{|\mathbf{r}-\mathbf{r}'-\mathbf{a}_{ij}-\mathbf{R}_p|}\,d\mathbf{r}\,d\mathbf{r}'\\&-2\sum_{i,j=1}^{N}\sum_{p=1}^{N_c}{}'\int_{\Omega_j}\frac{Z_i\rho^j(\mathbf{r})}{|\mathbf{r}-\mathbf{a}_{ij}-\mathbf{R}_p|}\,d\mathbf{r}\\&+\sum_{i,j=1}^{N}\sum_{p=1}^{N_c}{}'\frac{Z_iZ_j}{|\mathbf{a}_{ij}+\mathbf{R}_p|}.\end{aligned} \tag{9}$$

It should be noted that, even though $U_C$ is the energy per cell and its magnitude is proportional to $N$, it contains sums over an infinite number of atoms.

In the calculations to be described, $\rho^i(\mathbf{r}-\mathbf{a}_i-\mathbf{R}_p)$ has the muffin-tin form, which means that it is a spherically symmetric function $\rho^i_{\rm mt}(r)$ within a muffin-tin sphere of radius $R^i_{\rm mt}$ centered at $\mathbf{a}_i+\mathbf{R}_p$. It is a constant $\rho_0$ outside that sphere, but it goes to zero at the boundary of $\Omega_i$ as described above. It should be clear that, even in the muffin-tin case, $\rho^i(\mathbf{r}-\mathbf{a}_i-\mathbf{R}_p)$ is not a spherically symmetric function. Using the fact that the charge densities have the muffin-tin form and carrying out a considerable amount of manipulation leads to

$$U_C=\sum_{i,j=1}^{N}Q^i\alpha_{ij}Q^j-\sum_{i=1}^{N}[2\rho_0Q^i\gamma_i+\rho_0^2\Omega_i\gamma_i], \tag{10}$$

where

$$\alpha_{ij}=\sum_{p=1}^{\infty}{}'\frac{1}{|\mathbf{a}_{ij}+\mathbf{R}_p|}-\frac{1}{\Omega_C}\int\frac{d\mathbf{r}}{r}, \tag{11}$$

and

$$\gamma_i=\int_{\Omega_i}\frac{d\mathbf{r}}{r}. \tag{12}$$

The charges $Q^i$ are the integrals of the spherically symmetric function $\rho^i(\mathbf{r})-\rho_0\sigma^i(\mathbf{r})$, where $\sigma^i(\mathbf{r})$ is the step function that is one when $\mathbf{r}$ is in $\Omega_i$ and zero otherwise

$$Q^i=4\pi\int_0^{R^i_{\rm mt}}\rho^i_{\rm mt}(r)r^2dr-\rho_0\frac{4\pi}{3}(R^i_{\rm mt})3-Z_i. \tag{13}$$

The sum in Eq. (11) would not converge by itself, but it was pointed out by Ewald[15] that the inclusion of the integral over all space yields a convergent quantity. Techniques for calculating the Madelung constants $\alpha_{ij}$ on a computer are well developed.

The intra-atomic Coulomb interaction can be transformed into

$$\begin{aligned}U_C^i[\rho^i]=&2(4\pi)^2\int_0^{R_{\rm mt}}\rho^i_{\rm mt}(r)\int_0^r\rho^i_{\rm mt}(r')r'^2dr'r\,dr\\&-8\pi Z_i\int_0^{R_{\rm mt}}\rho^i_{\rm mt}(r)r\,dr-4\pi\rho_0Q^iR^2_{\rm mt}\\&-\frac{8\pi}{5}\rho_0^2\Omega^i_{\rm mt}R^2_{\rm mt}+[2\rho_0Q^i\gamma_i+\rho_0^2\Omega_i\gamma_i].\end{aligned} \tag{14}$$

It can be seen that, in the evaluation of $E_H[\rho]$, the terms included in the square brackets are canceled by the same terms in Eq. (10). The resulting expression for the Hartree energy per cell is the one that is normally used in band theory calculations on systems with more than one atom in a unit cell, and was first obtained by Asano and Yamashita.[16] Further details of the derivation can be found in that paper.

After the cancellation of the terms in the square brackets, the only contribution to the interatomic Coulomb energy is the sum, which can be written

$$\sum_{i,j=1}^{N}Q^i\alpha_{ij}Q^j=U_C^q+\sum_{i=1}^{N}(\rho_0^2\Omega_i-2\rho_0q^i)C^i, \tag{15}$$

where

$$C^i = \sum_{j=1}^{N} \alpha_{ij}\Omega_j . \tag{16}$$

The charge $q^i$ is the net charge in the atomic volume $\Omega_i$,

$$q^i = Q^i + \rho_0 \Omega_i . \tag{17}$$

These charges, which satisfy the neutrality condition,

$$\sum_{i=1}^{N} q^i = 0, \tag{18}$$

are the ones that will be defined as the charge associated with site $i$. The function $U_C^q$,

$$U_C^q = \sum_{i,j=1}^{N} q^i \alpha_{ij} q^j, \tag{19}$$

is formally equivalent to the interatomic Coulomb energy per cell of a series of point charges with magnitudes equal to the net charge per atomic cell $q^i$ placed on the sites $\mathbf{a}_i + \mathbf{R}_p$,

$$U_C^q = \sum_{i,j=1}^{N} \sum_{p=1}^{N_c}{}' \frac{q^i q^j}{|\mathbf{a}_{ij} + \mathbf{R}_p|}. \tag{20}$$

This result is obtained by treating the integral in Eq. (11) as a constant and making use of the neutrality condition of Eq. (18). It may also be written

$$U_C^q = \frac{1}{2} \sum_{i=1}^{N} q^i V^i, \tag{21}$$

where

$$V^i = \sum_{j=1}^{N} 2\alpha_{ij} q^j. \tag{22}$$

It is evident from these equations that, in the muffin-tin approximation, the interatomic Coulomb potential can be calculated as if the system is a lattice of point charges, even though the charge densities $\rho^i(\mathbf{r} - \mathbf{a}_i - \mathbf{R}_p)$ are not spherically symmetric. The reason for this is that $\rho(\mathbf{r}) - \rho_0$ can be written as a sum of nonoverlapping spherically symmetric charges, and the effect of the constant charge is taken care of by the integral that appears in the definition of the Madelung constants in Eq. (11). These equations are so useful that most treatments of the LDA equations start from them, even when the muffin-tin approximation is not used.

### B. Possible errors

It might be thought that the muffin-tin approximation would introduce unacceptable errors into these calculations. We argue that this is not the case because we are focusing on alloys of transition-metal alloys. A number of calculations[17] have shown that the muffin-tin approximation is quite good for transition metals. Reasons for this are that only a small fraction of the total charge is in the interstitial region outside the muffin-tin spheres, and that charge is uniformly distributed in that region.

When the points $\mathbf{a}_i + \mathbf{R}_p$ form a Bravais lattice, such as the fcc or bcc lattice, all the atomic volumes $\Omega_i$ are equal to $\Omega$ and $C^i$ in Eq. (16) is $A\Omega$, where

$$A = \sum_{j=1}^{N} \alpha_{ij} \tag{23}$$

is a constant independent of $i$. Then the interatomic Coulomb energy is simply $U_C^q$ plus a constant $NA\rho_0^2\Omega^2$. We assume that this is the case in the calculations to be discussed. It might seem that the displacement of the atoms about their ideal sites would complicate this picture because the atomic size of copper differs from that of zinc or palladium. The experimental evidence indicates that this is not the case for metallic alloys.

Atomic size effects have been studied by x-ray and neutron diffractionists for decades. The distortions due to size effects in homogeneous solid solution alloys are in the first class, according to the classification scheme of Krivoglaz,[18] which means that they produce a displacement of the Bragg peaks, a reduction in their intensity, and diffuse scattering. The Bragg peaks are not broadened. The displacement of the lines is simply related to the change in lattice constant of the alloy. A theory for the reduction in intensity of the Bragg peaks was developed by Krivoglaz, but there is experimental evidence that a simpler theory is quite adequate for metallic alloys.[19] In this theory, atomic displacements produce a reduction of the intensity of the Bragg peak located at the scattering angle $\theta$ by the factor $\exp[-2(B+B')\sin^2\theta/\lambda^2]$, where $B$ is the standard Debye-Waller factor and $B'$ is a static Debye-Waller factor. The mean square displacement of the atoms about their ideal sites due to the temperature-dependent excitation of phonons gives $B = \frac{8}{3}\pi^2\langle u_{\rm th}^2\rangle$, whereas the static displacement of the atoms caused by the size difference leads to $B' = \frac{8}{3}\pi^2\langle u_{\rm st}^2\rangle$. Since $B'$ is independent of temperature, $B$ and $B'$ can be found individually from powder-diffraction patterns measured at several temperatures.

For the case of an alloy with a very large size mismatch, copper-gold, it was found experimentally[20] that $B'$ is equal to $B$ at liquid-nitrogen temperatures and $B' = \frac{1}{3}B$ at room temperature. If copper and gold retained the sizes that they have in pure metals, $B'$ would have a value 20 times as large as the one observed. The size mismatch between copper and zinc is quite small, and, even for copper and palladium, these experimental observations indicate that static displacements will not affect the results of the calculations in this paper appreciably.

There are more sophisticated experimental studies of atomic size effects that can be carried out with x rays generated by a synchrotron, such as the 3λ measurements of the first moment of the mean static displacements of neighboring pairs of atoms in alloys.[21] It is an interesting challenge to construct a structural model that will reproduce the results of these experiments, but that model must also be consistent with the results of the much simpler experiments described above.

## III. CALCULATIONS

The equations in the preceding section have been used to calculate the electronic structure for models of substitutional alloys by setting up cells with $A$ and $B$ atoms on the sites of a bcc or fcc lattice. The total number of lattice sites is $N$, and the spatial distribution of the atoms is random in the sense

that the probability of an $A$ atom being on a site is $c$ and the probability of a $B$ atom being on the site is $1-c$.[22] These cells are periodically reproduced to fill all space, but the calculations cannot be done with conventional band theory methods because the computer time required for such calculations is proportional to $N^3$ and they are impractical for very large $N$. Methods for calculating the electronic structure of condensed matter have been developed recently which are known as order-$N$ methods because the computer times scale like $N$. Obviously, there must be some truncation of the fundamental equations to achieve this, but, in modern order-$N$ methods, the calculations are converged so that the truncation has no effect.

The order-$N$ method used here is called the locally self-consistent multiple-scattering (LSMS) method, and a complete description of this is in the literature.[23,24] It is based on the multiple-scattering equations of Rayleigh[25] that are also the basis for the Korringa, Kohn, Rostoker method.[26] It follows that the method is well-adapted to treat transition metals. When solving the multiple-scattering problem, the interaction of an atom with all neighbors in a local interaction zone that includes four or more nearest-neighbor shells is treated exactly. The Coulomb interactions with the remaining infinity of atoms are also treated exactly, but the multiple-scattering part is approximated. This process is repeated for each of the $N$ atoms in the cell, and the entire process is iterated until self-consistency is attained.

The calculations are speeded up by exploiting the analytic properties of the single-particle Green's function and the variational properties of the LDA, but they would be rather time consuming without a massively parallel supercomputer. The results of the self-consistent electronic structure calculation are expressed primarily in terms of the Green's function $G(E,\mathbf{r},\mathbf{r}')$. The density of one-electron states $n(E)$ is obtained from

$$n(E)=-\frac{1}{\pi}\lim_{z\to E}\ \mathrm{Im}\int G(z,\mathbf{r},\mathbf{r})d\mathbf{r}, \tag{24}$$

and the charge density of the electron gas at any point $\mathbf{r}$ in the sample is

$$\rho(\mathbf{r})=-\frac{1}{\pi}\ \mathrm{Im}\int_{-\infty}^{E_F}G(z,\mathbf{r},\mathbf{r})dz. \tag{25}$$

The net charges on the sites $q^i$ are calculated using Eqs. (13) and (17), and the Coulomb potentials $V^i$ at the sites are calculated from Eq. (22).

The LSMS is similar in philosophy to a method proposed recently by Kohn.[27] The use of a local interaction zone is equivalent to the principle of near sightedness described in that paper. The primary differences are that the LSMS makes no explicit use of the penalty function introduced in that paper, but it does include the long-range Coulomb interactions for all systems, not just the ionic crystals mentioned there.

### A. Results for a bcc copper-zinc alloy

The Coulomb potentials are plotted as a function of the net charges in Fig. 1 for a model of a 50% copper-zinc alloy with the nuclei placed on the ideal lattice sites of a body-centered cubic (bcc) crystal with a lattice constant of 5.5-bohr radii. The number of atoms $N$ in the cell for this calculation is 1024, so there are 512 $q^i,V^i$ points corresponding to copper sites and 512 corresponding to zinc sites. The atoms were distributed on the sites with the help of a random number generator. The charges associated with the copper sites are on the positive side of the figure because copper gains electrons from zinc, and the charge is measured in electron charges. It can be seen that $V^i$ is a linear function of the $q^i$, which is the $qV$ relation that was pointed out and discussed at some length in Refs. 7, 8, and 12. This relation is not simple electrostatics in that it does not exist for an arbitrary set of charges on the sites, even if the potentials are calculated exactly. The charges must be the result of a self-consistent LDA calculation. We observe this in our calculations during the approach to self-consistency. The system is neutral at every step, but there is a width to the distribution of the points about the line that becomes smaller as self-consistency is attained. The $qV$ relation for a 50% bcc copper-zinc alloy calculated with a cell that contains 256 atoms is also shown in Fig. 1. The agreement of the results from the two calculations shows that convergence is not a problem, a point that will be discussed in more detail in Sec. IV.

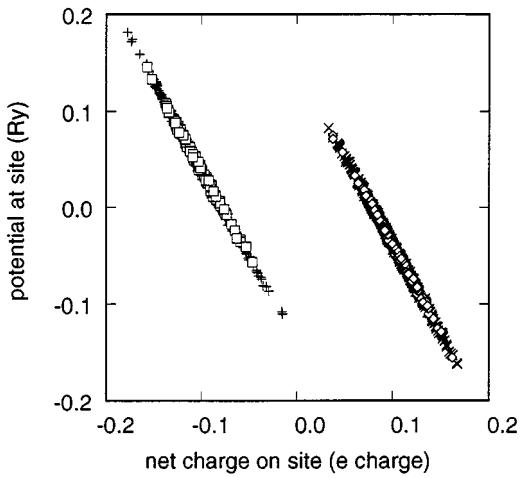


FIG. 1. The Coulomb potentials evaluated at the sites of a 50% bcc Cu-Zn alloy plotted against the net charge on the site. The 512 data points marked with crosses are for the sites occupied by Cu atoms in a model containing 1024 atoms in the cell, and the plus signs are for the Zn sites. The white diamond shapes are the 128 data points for the sites occupied by Cu atoms in a model containing 256 atoms, and the square shapes are for the Zn sites.

The sums that define the potentials $V^i$ do not converge at all rapidly. Since we have a table of all the charges in the sample described in the previous paragraph, we can study the convergence by calculating the contribution to $V^i$ from the atoms within and on the $n$th nearest-neighbor shell,

$$V^i(n)=\sum_{a_{ij}\le r_n}\frac{2q^j}{|\mathbf{a}_j-\mathbf{a}_i|}, \tag{26}$$

where the notation means that the only indices $j$ that are summed over are those for which $|\mathbf{a}_j-\mathbf{a}_i|\le r_n$, with $r_n$ the radius of the $n$th nearest-neighbor shell. The potential $V^i(n)$ for the site $i$ equal to 513, which happens to contain a Cu

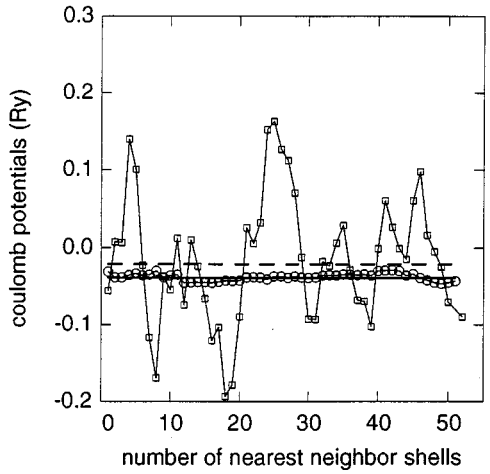


FIG. 2. The data points marked with squares connected by a solid line are the contributions to the Coulomb potential from charges included within $n$ nearest-neighbor shells $V^i(n)$. The potential shown is evaluated at site 513 in a 50% bcc Cu-Zn alloy that contains 1024 atoms in the cell. The straight dashed line shows the asymptotic value that $V^{513}(n)$ attains as $n\to\infty$. The data points marked with circles are the average of the $V^i(n)$ over all sites $i$ that contain Cu atoms. The straight solid line is the average $\langle V\rangle_{\mathrm{Cu}}$ of the Coulomb potentials at the Cu sites in the alloy.

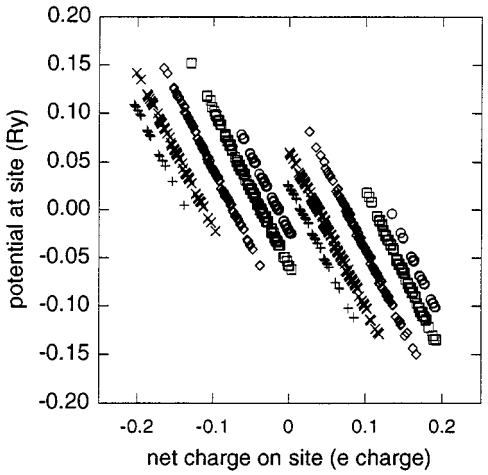


FIG. 3. The Coulomb potentials evaluated at the sites and the charges on the sites of fcc Cu-Zn alloys with cells containing 500 atoms. The plus signs for positive charges are the data points for sites containing Cu atoms and those in the negative region are for Zn atoms in an alloy with a Cu concentration of 90%. The crosses are for a 75% alloy, the diamonds for 50%, the squares for 25%, and the circles for 10% Cu.

atom, is plotted for $1<n<52$ in Fig. 2. (The reason that 52 shells are used in this plot is because the periodically reproduced central site is in the fifty-third nearest-neighbor shell for this 1024 atom model.) The behavior of $V^{513}(n)$ is typical of all the $V^i(n)$, and it can be seen that convergence to the value $V^{513}$ calculated for an infinite number of sites cannot be seen within a range of 52 nearest-neighbor shells. The average of the $V^i(n)$ for all sites $i$ that contain a Cu atom, $\langle V(n)\rangle_{\mathrm{Cu}}$, is compared with the average of the $V^i$,$\langle V\rangle_{\mathrm{Cu}}$, in Fig. 2 as well. It can be seen that approximate convergence is obtained for $n$ equal to one. This demonstrates the reliability of both calculations, and has other implications that will be discussed in Sec. IV.

A consequence of the charge neutrality condition of Eq. (18) is that the sum over all sites of the Coulomb potentials is zero

$$\sum_{i=1}^{N} V^i = 0. \tag{27}$$

Defining the average charge on the copper and zinc sites as $\langle q\rangle_{\mathrm{Cu}}$ and $\langle q\rangle_{\mathrm{Zn}}$, and the average potentials as $\langle V\rangle_{\mathrm{Cu}}$ and $\langle V\rangle_{\mathrm{Zn}}$, it follows from Eqs. (18) and (27) that

$$c\langle q\rangle_{\mathrm{Cu}} + (1-c)\langle q\rangle_{\mathrm{Zn}} = 0,$$

$$c\langle V\rangle_{\mathrm{Cu}} + (1-c)\langle V\rangle_{\mathrm{Zn}} = 0. \tag{28}$$

Dividing the second of these equations by the first, it follows that

$$\langle V\rangle_{\mathrm{Cu}} = -\alpha\langle q\rangle_{\mathrm{Cu}}, \quad \langle V\rangle_{\mathrm{Zn}} = -\alpha\langle q\rangle_{\mathrm{Zn}}. \tag{29}$$

The $qV$ relation illustrated in Fig. 1 can thus be expressed algebraically by the equations

$$V^i = -\beta_{\mathrm{Cu}}(q^i - \langle q\rangle_{\mathrm{Cu}}) - \alpha\langle q\rangle_{\mathrm{Cu}}, \quad i\subset \mathrm{Cu},$$

$$V^i = -\beta_{\mathrm{Zn}}(q^i - \langle q\rangle_{\mathrm{Zn}}) - \alpha\langle q\rangle_{\mathrm{Zn}}, \quad i\subset \mathrm{Zn}. \tag{30}$$

That these equations are an accurate representation of the results in Fig. 1 is demonstrated by the fact that, in a least-squares fit to the calculated data, the rms deviation is very small and there is no improvement to the fit when terms quadratic in the fluctuations $(q^i-\langle q\rangle_{\mathrm{Cu}})$ or $(q^i-\langle q\rangle_{\mathrm{Zn}})$ are added to the fitting functions. There is no requirement that the slopes $\beta_{\mathrm{Cu}}$ and $\beta_{\mathrm{Zn}}$ must be the same, although it is clear from Fig. 1 that the difference is small.

### B. Results for fcc copper-zinc alloys

The Coulomb potentials are plotted as a function of the net charges in Fig. 3 for copper-zinc alloys that have the face-centered (fcc) crystal structure and copper concentrations of 10%, 25%, 50%, 75%, and 90%. Five hundred atoms are randomly distributed on the ideal lattice positions, and the lattice constant of 6.90-bohr radii is used for all concentrations. The data fall on a series of straight lines that are approximately parallel, as described in Eq. (30). The parameters $\alpha$, $\beta_{\mathrm{Cu}}$, and $\beta_{\mathrm{Zn}}$ have a weak concentration dependence that is shown in Fig. 4. The midpoints of the lines are the $\langle V\rangle_{\mathrm{Cu}}$, $\langle q\rangle_{\mathrm{Cu}}$ and $\langle V\rangle_{\mathrm{Zn}}$, $\langle q\rangle_{\mathrm{Zn}}$ points appropriate for the given concentration. The displacement of the lines relative to each other is determined by the charge neutrality conditions in Eq. (28) and the parameter $\alpha$.

It can be seen that the lines for the extreme concentrations, 10% or 90%, are broken up into segments and appear to be shorter than those for intermediate concentrations. This is due to the finite number of atoms in our cells. For an infinite crystal, the spaces will be filled in and the lines will appear continuous. It will still be the case that the density of points along the line is not uniform, however. The reasons for this and also for the concentration dependence of $\alpha$, $\beta_{\mathrm{Cu}}$, and $\beta_{\mathrm{Zn}}$ are discussed in Sec. IV.

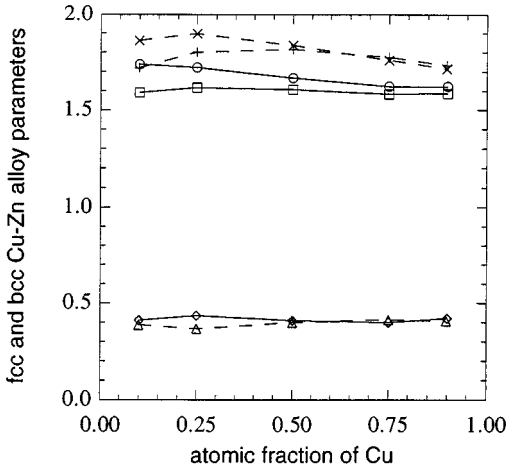


FIG. 4. The parameters that determine the relation between charges and Coulomb potentials in Cu-Zn alloys. The models for the fcc alloys have cells that contain 500 atoms and those for bcc alloys contain 432 atoms. The solid lines connect the values for the fcc alloys, the circles indicating the values for $\beta_{\mathrm{Cu}}$, the squares for $\beta_{\mathrm{Zn}}$, and the diamonds for $\alpha$. The dashed lines connect the values for the bcc alloys, the crosses indicating the values for $\beta_{\mathrm{Cu}}$, the plus signs for $\beta_{\mathrm{Zn}}$, and the triangles for $\alpha$.

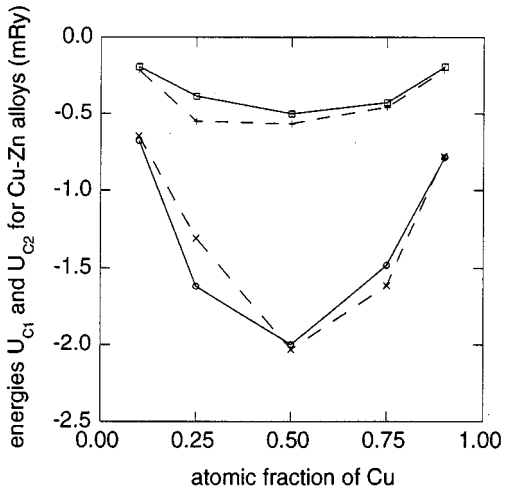


FIG. 5. The contributions to the Coulomb energy $u_{C1}$ and $u_{C2}$ for Cu-Zn alloys. The models for the fcc alloys have cells that contain 500 atoms and those for bcc alloys contain 432 atoms. The solid lines connect the values for the fcc alloys, the circles indicating the values for $u_{C1}$ and the squares for $u_{C2}$. The dashed lines connect the values for the bcc alloys, the crosses indicating the values for $u_{C1}$ and the plus signs for $u_{C2}$.

### C. Coulomb energies of copper-zinc alloys

The interatomic Coulomb energy per atom $u_C^q = U_C^q/N$ obtained by inserting Eq. (30) into Eq. (21) is

$$u_C^q = u_{C1} + u_{C2}, \tag{31}$$

where

$$u_{C1} = \alpha \tfrac{1}{2} \langle q \rangle_{\mathrm{Cu}} \langle q \rangle_{\mathrm{Zn}},$$

$$u_{C2} = -\beta_{\mathrm{Cu}} \frac{c}{2N_{\mathrm{Cu}}} \sum_{i \subset \mathrm{Cu}}^{N_{\mathrm{Cu}}} (q^i - \langle q \rangle_{\mathrm{Cu}})^2 - \beta_{\mathrm{Zn}} \frac{1-c}{2N_{\mathrm{Zn}}} \sum_{i \subset \mathrm{Zn}}^{N_{\mathrm{Zn}}} (q^i - \langle q \rangle_{\mathrm{Zn}})^2. \tag{32}$$

The form of this equation for $u_C^q$ has some interesting implications for the DFT-LDA theory, as was discussed in Ref. 12. The first term $u_{C1}$ depends only on the average charges, while $u_{C2}$ depends on the mean-square deviations from the average charges. These two parts of the Coulomb energy are plotted as a function of concentration in Fig. 5 for the fcc alloys described above. Since $u_C^q(c)$ must be zero for $c=0$ and 1, it is not surprising that these curves are roughly parabolic.

LSMS calculations on models of bcc copper-zinc alloys with $N$ equal to 432 and copper concentrations of 10%, 25%, 50%, 75%, and 90% have been described in Refs. 8 and 12. The lattice constant used in all of those calculations is the same as the one used for the calculation done with 1024 atoms described above, 5.5-bohr radii. For the lattice constants we have used, the Wigner Seitz radius for the fcc lattice is 2.697-bohr radii, and for the bcc lattice it is 2.708-bohr radii. The Coulomb energies $u_{C1}$ and $u_{C2}$ for these alloys are also plotted in Fig. 5. This figure demonstrates that the Coulomb energies in alloys depend surprisingly little on structure. Of course, copper and zinc atoms are almost the same size and their atomic volumes are about the same in a bcc or fcc alloy. The charge per site transferred from the zinc to the copper sites,

$$\Delta = \langle q \rangle_{\mathrm{Cu}} - \langle q \rangle_{\mathrm{Zn}}, \tag{33}$$

depends very little on concentration and is approximately the same for the two structures. The binding energy of alloys is typically of the order of hundreds of milli-Rydbergs and the difference in energy between two phases for a given alloy is typically of the order of milli-Rydbergs. The energy $u_C^q$ is about 2.5 mRy for both the fcc and bcc alloys, so the magnitude of these Coulomb energies is not insignificant. However, their importance is diminished by their insensitivity to structure.

The details of the dependence of $u_{C1}$ and $u_{C2}$ on concentration is related to the concentration dependence of the $\alpha$, $\beta_{\mathrm{Cu}}$, and $\beta_{\mathrm{Zn}}$. We have commented on the plots of those functions for the fcc alloys shown in Fig. 4. We plot them for the bcc alloys in the same figure.

### D. Results for fcc copper-palladium alloys

These calculations on the copper-zinc alloy system illustrate the concentration and structure dependence of $u_C^q(c)$, but it might be thought that they are specific to this system. For that reason, calculations on a system that is known to be qualitatively very different, the copper palladium system, have been carried out. In the neighborhood of the Fermi energy, the electronic states for both copper and zinc, and any alloy of these two metals, are primarily $s$-$p$ states. The electronic states for palladium, on the other hand, have sig-

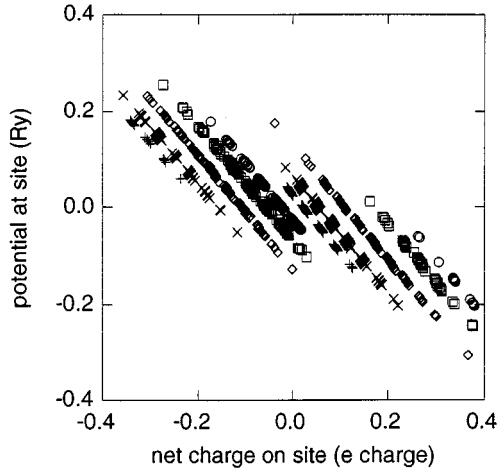


FIG. 6. The Coulomb potentials evaluated at the sites and the charges on the sites of fcc Cu-Pd alloys with cells containing 256 atoms. The plus signs for positive charges are the data points for sites containing Cu atoms and those in the negative region are for Pd atoms in an alloy with a Cu concentration of 90%. The crosses are for a 75% alloy, the diamonds for 50%, the squares for 25%, and the circles for 10% Cu.

nificant $d$ character, and it follows that the density of states at the Fermi energy for palladium atoms will be much larger than that for either copper or zinc.

The Coulomb potentials are plotted as a function of the net charges in Fig. 6 for models of copper-palladium alloys with the fcc crystal structure having concentrations of 10%, 25%, 50%, 75%, and 90%. Two hundred and fifty-six atoms are randomly distributed on the ideal lattice positions, and the lattice constant 7.1-bohr radii is used for all concentrations. It can be seen that the linear $qV$ relation is displayed by this alloy as clearly as it is for the copper-zinc alloys. The slopes $\alpha$, $\beta_{\mathrm{Cu}}$ and $\beta_{\mathrm{Pd}}$ are plotted in Fig. 7 as a function of concentration. By comparing this figure with Fig. 4, it can be seen that $\beta_{\mathrm{Cu}}$, and $\beta_{\mathrm{Pd}}$ are significantly smaller than the slopes for the Cu-Zn alloys, and they have significantly less

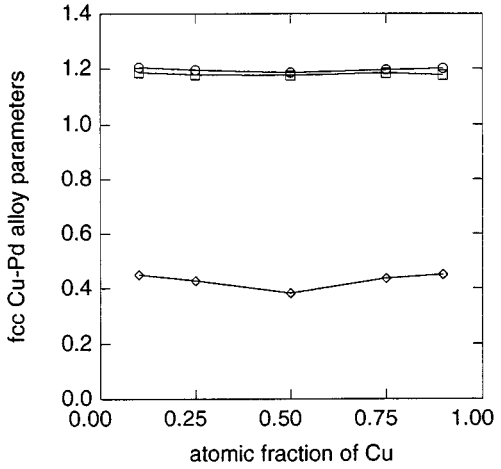


FIG. 7. The parameters that determine the relation between charges and Coulomb potentials in fcc Cu-Pd alloys calculated with cells that contain 256 atoms. The circles indicate the values for $\beta_{\mathrm{Cu}}$, the squares for $\beta_{\mathrm{Pd}}$, and the diamonds for $\alpha$.

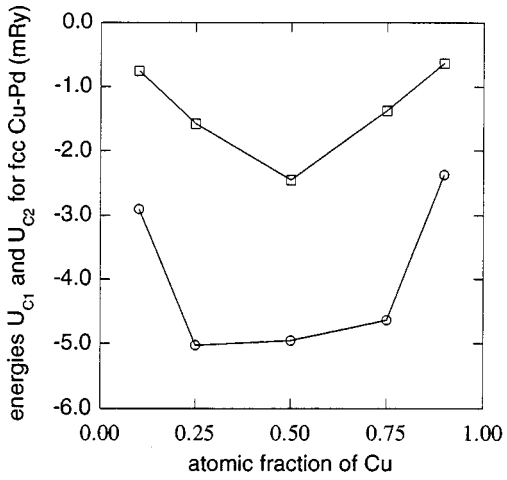


FIG. 8. The contributions to the Coulomb energy $u_{C1}$ and $u_{C2}$ for fcc Cu-Pd alloys with cells that contain 256 atoms. The circles indicate the values for $u_{C1}$ and the squares for $u_{C2}$.

concentration dependence. Also, $\beta_{\mathrm{Cu}}$ and $\beta_{\mathrm{Pd}}$ are less different from each other than $\beta_{\mathrm{Cu}}$ and $\beta_{\mathrm{Zn}}$, which is somewhat surprising.

The two contributions to the Coulomb energy $u_{C1}$ and $u_{C2}$ are shown if Fig. 8 for these alloys. They have the expected approximately parabolic shape, but the maximum magnitude is significantly greater. This is due to a larger charge exchange between the copper and palladium sites. The differences between the average charges on the Cu and Zn sites in the fcc and bcc Cu-Zn alloys are plotted as a function of concentration in Fig. 9, and compared with the corresponding $\Delta$'s for the fcc Cu-Pd alloys.

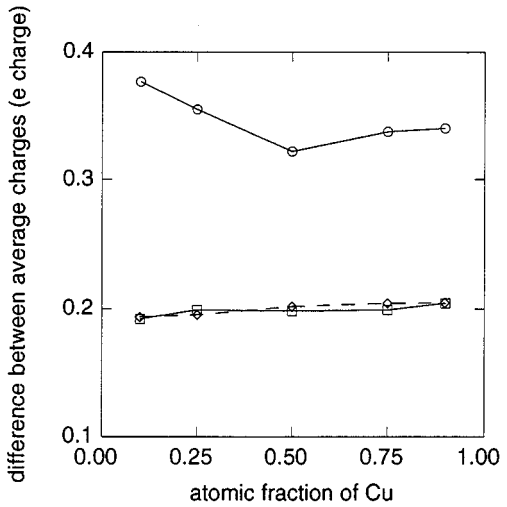


FIG. 9. The differences between the average charges on the atoms of the two constituents in random alloys. The differences between $\langle q\rangle_{\mathrm{Cu}}$ and and $\langle q\rangle_{\mathrm{Pd}}$ in fcc Cu-Pd alloys calculated with cells that contain 256 atoms are indicated by circles. The differences between $\langle q\rangle_{\mathrm{Cu}}$ and $\langle q\rangle_{\mathrm{Zn}}$ in models of fcc Cu-Zn alloys calculated with cells that contain 500 atoms are indicated by squares. The differences between $\langle q\rangle_{\mathrm{Cu}}$ and $\langle q\rangle_{\mathrm{Zn}}$ in models of bcc Cu-Zn alloys calculated with cells that contain 432 atoms are indicated by diamonds.

## IV. THEORETICAL CONSIDERATIONS

### A. The parameter $\alpha$

The first topic to be considered in this section is a derivation that explains the origin and the approximate magnitude of the parameter $\alpha$ introduced in Eq. (29). For this part of the discussion, it is convenient to write the net charge on a site as $q(\mathbf{a}_i)$ rather than $q^i$. The average $\langle q(0)q(\mathbf{a}_k)\rangle$ is defined by

$$\langle q(0)q(\mathbf{a}_k)\rangle = \frac{1}{N}\sum_{i=1}^{N} q(\mathbf{a}_i)q(\mathbf{a}_i+\mathbf{a}_k), \tag{34}$$

and is called the charge-charge correlation function. Because of the neutrality of the crystal, this correlation function satisfies the sum rule,

$$\sum_{k=1}^{N} \langle q(0)q(\mathbf{a}_k)\rangle = 0. \tag{35}$$

It might be worth pointing out at this point that the averages that are written as sums over sites in this paper are equivalent to ensemble averages if the system is big enough. Since we are invoking charge neutrality, the canonical ensemble made up of all systems with a fixed number of Cu and Zn atoms should be used.

Starting from the formula in Eq. (26) for the Coulomb shift at the $i$th site due to charges within and on the $n$th nearest-neighbor shell, a formula for the average of these potentials can be written

$$\langle V(n)\rangle_{\mathrm{Cu}} = \sum_k{}' \ \frac{2\langle q(\mathbf{a}_k)\rangle_{\mathrm{Cu}}}{a_k},$$

$$\langle V(n)\rangle_{\mathrm{Zn}} = \sum_k{}' \ \frac{2\langle q(\mathbf{a}_k)\rangle_{\mathrm{Zn}}}{a_k}. \tag{36}$$

The primes on the summation signs mean that the sum is only over sites such that $a_k < r_n$, the radius of the $n$th nearest-neighbor shell, and the restricted averages introduced in this formula are defined by

$$\langle q(\mathbf{a}_k)\rangle_{\mathrm{Cu}} = \frac{1}{N_{\mathrm{Cu}}}\sum_{i\subset \mathrm{Cu}}^{N_{\mathrm{Cu}}} q(\mathbf{a}_i+\mathbf{a}_k),$$

$$\langle q(\mathbf{a}_k)\rangle_{\mathrm{Zn}} = \frac{1}{N_{\mathrm{Zn}}}\sum_{i\subset \mathrm{Zn}}^{N_{\mathrm{Zn}}} q(\mathbf{a}_i+\mathbf{a}_k). \tag{37}$$

The sites summed over in the calculation of $\langle q(\mathbf{a}_k)\rangle_{\mathrm{Cu}}$ are not necessarily occupied by Cu atoms, the notation is meant to indicate that the site $\mathbf{a}_i$ is occupied by a Cu atom. These restricted averages are similar to the charge-charge correlation function of Eq. (34), and also obey sum rules that are the analog of Eq. (35),

$$\sum_{k=1}^{N} \langle q(\mathbf{a}_k)\rangle_{\mathrm{Cu}} = 0, \quad \sum_{k=1}^{N} \langle q(\mathbf{a}_k)\rangle_{\mathrm{Zn}} = 0. \tag{38}$$

Our LSMS data was used to calculate the restricted averages for the alloy samples described in this paper, and the evidence is that they are approximately zero when the magnitude $a_k$ is greater than the radius of the first nearest-neighbor shell $r_1$. This has already been illustrated in Fig. 2, because it is equivalent to the observation that $\langle V(n)\rangle_{\mathrm{Cu}} \approx \langle V\rangle_{\mathrm{Cu}}$ and $\langle V(n)\rangle_{\mathrm{Zn}} \approx \langle V\rangle_{\mathrm{Zn}}$ for $n>1$. It follows that

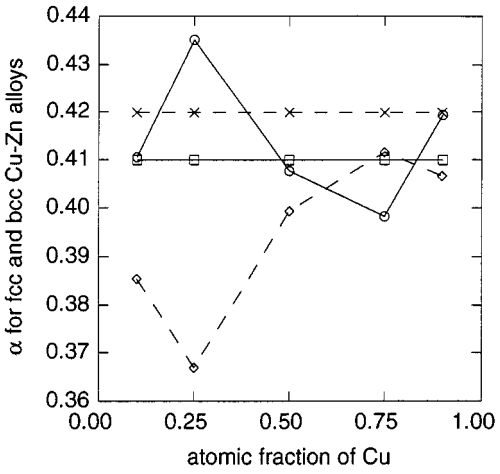


FIG. 10. A comparison of the parameters $\alpha$ with $2.0/r_1$ for Cu-Zn alloys. The circles are the $\alpha$'s and the squares $2.0/r_1$ for fcc alloys calculated with 500 atoms in the cell, and the points are connected by solid lines. The diamonds are the $\alpha$'s and the crosses $2.0/r_1$ for fcc alloys calculated with 500 atoms in the cell, and the points are connected by dashed lines.

$$\sum_{a_k \geqslant r_1} \langle q(\mathbf{a}_k)\rangle_{\mathrm{Cu}} = -\langle q\rangle_{\mathrm{Cu}}, \quad \sum_{a_k \geqslant r_1} \langle q(\mathbf{a}_k)\rangle_{\mathrm{Zn}} = -\langle q\rangle_{\mathrm{Zn}}, \tag{39}$$

and the average shifts $\langle V\rangle_{\mathrm{Cu}}$ and $\langle V\rangle_{\mathrm{Zn}}$ are given by

$$\langle V\rangle_{\mathrm{Cu}} = -\frac{2\langle q\rangle_{\mathrm{Cu}}}{r_1}, \quad \langle V\rangle_{\mathrm{Zn}} = -\frac{2\langle q\rangle_{\mathrm{Zn}}}{r_1}. \tag{40}$$

This derivation leads to the prediction that the parameter $\alpha$ is equal to $2/r_1$. The values of $\alpha$ are plotted in Fig. 10 for the fcc and bcc Cu-Zn alloys. It can be seen that they are rather close to $2/r_1$ for the fcc alloys. The true values for $\alpha$ are consistently smaller than $2/r_1$ for the bcc alloys, which means that the correlation length is larger than $r_1$ for these alloys. The values of $\alpha$ are plotted in Fig. 11 for the Cu-Pd alloys. The difference between the calculated values and the approximation is greater for this more highly charged alloy. It should be emphasized that Eq. (40) is basically a consequence of the overall charge neutrality of the crystal and the correlation length of the charges. The only sense in which this equation could be interpreted as describing the screening of the central charge by charges on the first-nearest-neighbor shell is by focusing on a mathematical abstraction, the average copper or zinc site. The screening of any actual site in the alloy is illustrated by the function $V^i$ in Fig. 2.

### B. The slopes $\beta$

We will now consider the slopes $\beta$ that were introduced in Eq. (30). Introducing parameters $\gamma$ that are the reciprocals of the $\beta$'s makes it possible to rewrite Eq. (30) in the form

$$(q^i - \langle q\rangle_{\mathrm{Cu}}) = -\gamma_{\mathrm{Cu}}(V^i - \langle V\rangle_{\mathrm{Cu}}),$$

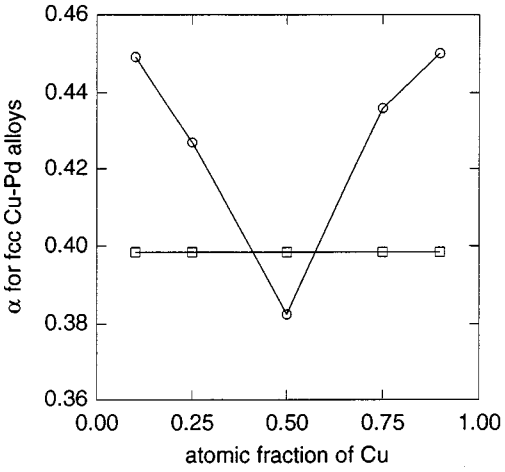


FIG. 11. A comparison of the parameters $\alpha$ with $2.0/r_1$ for fcc Cu-Pd alloys calculated with 256 atoms in the cell. The circles are the $\alpha$'s and the squares are $2.0/r_1$.

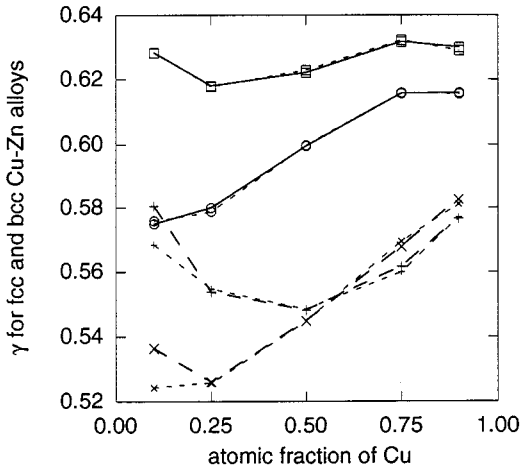


FIG. 12. The slopes $\gamma_{Cu}=1/\beta_{Cu}$ and $\gamma_{Zn}=1/\beta_{Zn}$ for fcc and bcc Cu-Zn alloys. The circles represent the values for $\gamma_{Cu}$ and the squares for $\gamma_{Zn}$ for the fcc alloys. The line made up of short dashes connects the data points for the approximate values obtained from Eq. (42) with the constants written below that equation. The crosses represent the values for $\gamma_{Cu}$ and the plus signs for $\gamma_{Zn}$ for the bcc alloys. The line made up of short dashes connects the data points for the approximate values obtained from Eq. (42).

$$(q^i-\langle q\rangle_{Zn})=-\gamma_{Zn}(V^i-\langle V\rangle_{Zn}). \tag{41}$$

Clearly the $\gamma$'s describe the rate at which the charge will be induced on a site by the Coulomb potential at that site. It is reasonable to expect that this rate will be related to the density of states at the Fermi energy for the atom. The fact that the slopes of the $qV$ lines are characteristic of an alloy at a given concentration, as seen in Figs. 4 and 7, suggests that the $\gamma$'s should be related to the average densities of states at the Fermi energy at that concentration, $\langle\rho\rangle_{Cu}$ and $\langle\rho\rangle_{Zn}$. The densities of states at the Fermi energy for all the atoms in our samples, as well as their averages, can been obtained readily from our LSMS calculations.

The simplest relationship that the $\gamma$'s can have with the average density of states is linear, so we attempted to fit them to the functions

$$\gamma_{Cu}=a_{Cu}+b_{Cu}\langle\rho\rangle_{Cu},\quad \gamma_{Zn}=a_{Zn}+b_{Zn}\langle\rho\rangle_{Zn}. \tag{42}$$

Our best fits for the fcc alloys described in Sec. III B lead to the values, $a_{Cu}=0.231\,58$, $b_{Cu}=0.092\,73$, $a_{Zn}=0.238\,32$, and $b_{Zn}=0.128\,85$. Our best fits for the bcc alloys described in Refs. 8 and 12 lead to $a_{Cu}=0.207\,22$, $b_{Cu}=0.089\,39$, $a_{Zn}=0.232\,91$, and $b_{Zn}=0.114\,98$. The values for $\gamma$ calculated from our LSMS data are plotted in Fig. 12, and compared with values calculated from Eq. (42). It can be seen that the agreement for the fcc alloys is excellent and for the bcc alloys it is quite good. The worst agreement is for the bcc alloy with 10% Cu. (When we saw this, we repeated the calculation for another 10% alloy generated in the same way. The slope $\gamma_{Cu}$ changed from 0.536 51 to 0.536 65, while $\gamma_{Zn}$ changed from 0.580 49 to 0.590 81, amounts that are inconsequential.) It should be emphasized that the $a$'s and $b$'s are independent of concentration, so that the concentration dependence of the $\gamma$'s, and hence the slopes of the lines in Figs. 1, 3, and 6 are due to the concentration dependence of the average densities of states $\langle\rho\rangle_{Cu}$ and $\langle\rho\rangle_{Zn}$.

The relation between $\gamma$ and the density of states should not lead to the conclusion that the $qV$ relation is simply caused by the charge flowing onto a site due to a displaced potential. In the first place, the displacement of a potential is not simply related to the Coulomb shift. A rigid displacement of a potential is reflected in a shift of the core levels. The displacement of the $1S$ core levels of copper and zinc from there average values on the sites of a 50% bcc alloy is plotted in Fig. 13 versus the Coulomb potential at the site. Drawing lines through the data points, it can be calculated that a shift of the Coulomb potential leads to a shift of the potential that is roughly 0.2474 times as large for the zinc atoms and 0.2856 times as large for the copper atoms. This is due to screening by the outer electrons, and is not surprising. It is more important to note that there is considerably more scatter in the data points about the straight line than there is in the $qV$ plots. This fact, plus the fact that the slopes $\gamma_{Cu}$

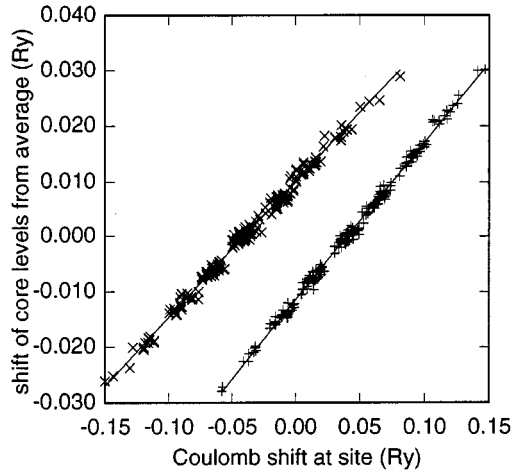


FIG. 13. The shifts of the $1S$ core levels from their average values versus the Coulomb potential at the sites in an fcc Cu-Zn alloy with a concentration of 50% calculated with a sample that contains 500 atoms. The crosses are for the Cu atoms and the plus signs are for the Zn atoms.

and $\gamma_{\mathrm{Zn}}$ are more nearly the same than would be expected from a potential shift argument, indicates that such an argument cannot explain the $qV$ relation.

The preceding derivations allow us to make reasonable predictions for the dependence of the parameters in Eq. (30) on the concentration and the atomic species. This is far from a complete theory, since the only way that we can get the constants that appear in Eq. (42) is from the LSMS calculations. As pointed out in Ref. 12, a more complete analysis must be based on the DFT-LDA equations in Sec. II, making use of the concept of fragments introduced by Harris.[28] The analysis is quite complicated because of the long-range nature of the Coulomb potentials and the global adjustment of the Fermi energy that is necessary for charge neutrality.

### C. Extrapolation to macroscopic samples

It should be emphasized that all the work that we have done on this problem is based on the fundamental assumption that there is a well-defined state of matter that can be called a disordered alloy with concentrations of the constituents $c$ and $1-c$, and that the physical properties of such an alloy do not vary from sample to sample. The ideal alloy can be modeled theoretically by distributing atoms randomly on an infinite set of lattice points with probabilities $c$ and $1-c$, and can be fabricated experimentally by annealing certain metallic alloys at high temperature and then rapidly quenching them.

The short-range order in an alloy is usually described in terms of the Warren-Cowley short-range-order (SRO) parameters,[29]

$$\alpha_{1mn}=1-\frac{1}{2c(1-c)}\,P_{lmn}\{A|B\}, \tag{43}$$

where $P_{lmn}\{A|B\}$ is the probability for finding an $A$ atom on the specified nearest-neighbor shell if it is known that there is a $B$ atom at the origin. For historical reasons, the nearest-neighbor shells are specified by Miller indices. If there is a tendency for unlike atoms to be neighbors, short-range ordering,

$$-\left(\frac{1}{2c(1-c)}-1\right)<\alpha_{lmn}<0, \tag{44}$$

while

$$0<\alpha_{lmn}<1, \tag{45}$$

for the opposite case of short-range clustering. In the ideal disordered alloy, all of the SRO parameters are zero.

An intermetallic compound can be fabricated by annealing certain alloys that have a specific concentration for a long period of time at a temperature just below the ordering temperature. It is a long-range-ordered structure with a relatively small number of atoms in the unit cell and symmetry that is described by one of the tabulated space groups. It is possible to model a disordered alloy with periodic boundary conditions as an intermetallic compound in the limit as the number of atoms in the unit cell $N$ approaches infinity, as has been done in the calculations described in this paper.

Many characteristics of a disordered alloy are qualitatively different from those of an intermetallic compound. This proposition seems self-evident, but, when modeling the alloy with supercells, the question is, how large does $N$ have to be? The theoretical proposition that the divergence in the properties must take place somewhere between the microscopic and macroscopic limit has been argued persuasively by Anderson, who also supplied a number of examples from his research interests.[30] A simple example of a property that demonstrates this qualitative difference is the finite residual resistivity of a disordered alloy, which is the electrical resistivity of an alloy in the limit as the temperature approaches zero. An ordered intermetallic compound will have a resistivity at $T=0$ that is zero or infinity. A less simple example is Anderson localization.[31] A correct calculation of the residual resistivity using supercells containing thousands of atoms would still lead to zero or infinity, and there can clearly be no localization in a periodically reproduced system. However, using a proper formulation of the theory, calculations with supercells no larger than the ones in this paper have produced some remarkably good predictions for both of these properties.[32] Anderson argues, quite correctly, that many properties of the infinite system cannot be seen in the results of calculations on finite clusters. At the same time, the conclusion drawn in the work that we just alluded to and from our own experience is that, using a combination of physical insight and calculations on large clusters, one can obtain correct extrapolations to the properties of the disordered alloy.

As an example of the application of this proposition to Coulomb effects, extrapolating the calculations in this paper leads to the conclusion that the disordered alloy will have a continuous distribution of magnitudes of the charges $q^i$. In the calculations that we have done on samples of different sizes, we have yet to find two charges with the same magnitude in the same sample. It follows from the $qV$ relation that their is also a continuous distribution of Coulomb potentials $V^i$. We will demonstrate that the convergence of our calculations is sufficient so that we can have confidence in our extrapolations to macroscopic ideal alloys.

### D. Convergence of the calculations

In the early days of alloy theory, Lifshitz argued on intuitive grounds that one can calculate the properties of a disordered alloy from one sufficiently large sample,[33] and referred to this property of a large sample as self-averaging. It can be seen most easily in exact calculations of the electron or phonon density of states of finite one-dimensional models of disordered alloys.[34] Calculations on simplified three-dimensional models show the same effect.[35] Practical tests for the self-averaging property of samples used in calculations are that the quantities computed (a) change little as the sizes of the samples are increased, and (b) are essentially the same for different samples of the same size constructed according to a specified prescription. We applied the tests described above to ascertain if the models that we used in our calculations are self-averaging.

We carried out calculations on models of the 50% bcc Cu-Zn alloy with 256, 432, and 1024 atoms. The models have the same lattice spacing, and the atoms were placed on the sites with equal probabilities using a random number generator. The total energies per atom for the 256, 432, and 1024 atom samples are $-3414.461\,44$, $-3414.461\,14$, and

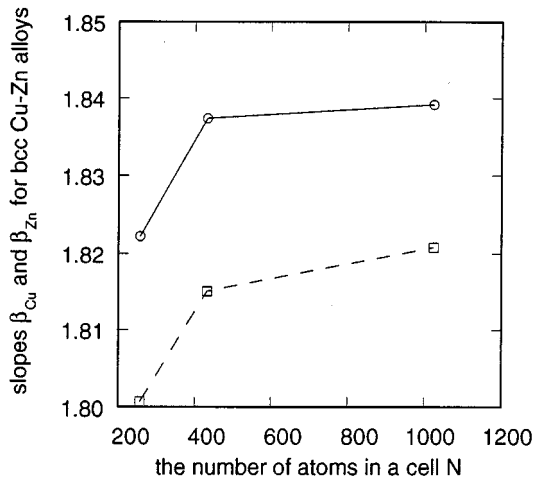


FIG. 14. The slopes $\beta_{Cu}$ (circles) and $\beta_{Zn}$ (squares) of the lines on which the data points fall in Fig. 1. The slopes are calculated for models of a 50% bcc Cu-Zn alloy with cells that contain 256, 432, and 1024 atoms.

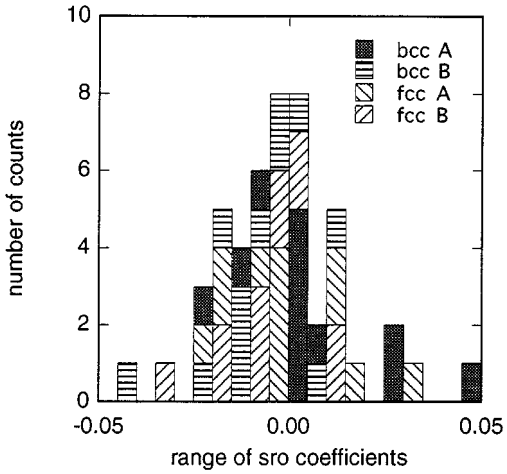


FIG. 15. A stacked histogram that shows the distribution of the Warren-Cowley short-range-order coefficients corresponding to the first 12 nearest-neighbor shells for four 50% Cu-Zn alloys. The fcc samples contain 500 atoms and the bcc samples contain 432 atoms.

−3414.461 09 Ry. The Coulomb potentials are plotted as a function of the net charges in Fig. 1 for two of these samples, and it is evident from that drawing that the slopes change very little. We calculated the slopes $\beta_{Cu}$ and $\beta_{Zn}$ for these samples, and have plotted them in Fig. 14 as a function of the number of atoms in the sample. It can be seen that there is only a 1% difference between the slopes calculated with the smallest and the largest sample. All of this data indicates that the properties that we are focusing on can be obtained reliably from samples with as few as 256 atoms in them.

We carried out calculations on pairs of samples with 432 atoms of the 50% bcc Cu-Zn alloy and samples with 500 atoms of the 50% fcc alloy. Different seeds were used in the random number generator, so there is no relation between the positions of the atoms in the pairs of samples. As with all of our alloy samples, part of the calculation is to obtain the Warren-Cowley SRO parameters defined in Eq. (43) for the first 12 nearest-neighbor shells. A statistical analysis of all of these parameters is shown in Fig. 15. It can be seen that they cluster around zero, with two of the 48 parameters being as large as 0.05. These maximum values are for the fourth shell in one sample and the sixth in another sample. Experimentally, an alloy is considered to be disordered when it has SRO parameters for the first shell as large as 0.20.[36] It is mathematically possible to calculate the probability for the SRO parameters being unacceptably large for a give sample. We have not done this, but, in all of the samples that we have generated to date, we have not had to reject one because the SRO parameters were larger than 0.05.

We list in Table I a set of calculated parameters for the four samples described in the previous paragraph. The differences in the parameters for these samples that have completely different arrangements of atoms are very small. We feel that this table provides further evidence that our samples are self-averaging.

### E. The magnitudes of the charges

As stated in Sec. IV C, the extrapolation of these calculations leads to the conclusion that the distribution of magnitudes of the charges in a disordered alloy is continuous. That is not to say, however, that the distribution of the charges is uniform. The probability $P_{Cu}(c,q)$ for a copper atom in a fcc disordered Cu-Zn alloy with the concentration $c=0.50$ to have a charge between $q$ and $q+0.005$ electron charges is shown in Fig. 16. It is calculated with the charges from the model of the 50% alloy that was described in Sec. III B, which contains 250 Cu and 250 Zn atoms. It can be seen that the distribution of charges about the average value is not uniform. It is easier to study the distribution of charges if one does not concentrate on alloys with just one concentration.

The probability $P_{Cu}(q)$ for a copper atom in a fcc disordered alloy to have a charge between $q$ and $q+0.005$ electron charges is calculated from the data on such alloys in Sec. III B and plotted in Fig. 17. It does not depend on the concentration $c$ since the charges from all five concentrations, ranging from 10% to 90%, are lumped together in the calculation to approximate the integral of the $P_{Cu}(c,q)$ over $c$. This is justified because the same lattice constant was used for all concentrations. The function $P_{Cu}(q)$ has thirteen well-defined peaks. The conditional probability $P_{Cu}(f_1,q)$, which is the probability that a Cu atom in a fcc disordered Cu-Zn alloy that has a fraction $f_1$ of Cu atoms on the first-nearest-neighbor shell will have a charge between $q$ and $q+0.005$, is also shown in Fig. 17 for the case $f_1=1/2$. The number of Zn atoms in the nearest-neighbor shell, introduced in Eq. (43), is $n_{Zn}=n_1(1-f_1)$, where $n_1$ is the number of atoms in that shell. For a fcc crystal, $n_1=12$. Since $P_{Cu}(q)$ is a superposition of the thirteen functions $P_{Cu}(f_1,q)$ that correspond to the integer values for $n_{Zn}$ from 0 to 12, it is obvious that this is the origin of the structure in $P_{Cu}(q)$. We feel that our statistical sample is large enough so that the general features of $P_{Cu}(q)$ are reliable, although the relative heights of the peaks in different regions of charge may be changed by more data.

Clearly the ability to predict the value of the charge $q$ of a given Cu atom is improved significantly by the knowledge of the environment of the atom as described by the fraction $f_1$, but there is still a considerable uncertainty that is given

TABLE I. The total energy per atom and parameters defined in Eqs. (33), (31), (29), and (30) for four 50% Cu-Zn alloys. The two fcc samples contain 500 atoms and the two bcc samples contain 432 atoms.

| | Total energy | $\Delta$ | $u_C^q$ | $\alpha$ | $\beta_{Cu}$ | $\beta_{Zn}$ |
|---|---|---|---|---|---|---|
| fcc *A* | −3414.460 52 | 0.198 13 | −2.501 26 | 0.407 61 | 1.665 16 | 1.605 99 |
| fcc *B* | −3414.460 53 | 0.198 61 | −2.602 80 | 0.410 14 | 1.664 84 | 1.606 40 |
| bcc *A* | −3414.460 90 | 0.197 21 | −2.457 86 | 0.363 59 | 1.832 18 | 1.820 54 |
| bcc *B* | −3414.461 14 | 0.200 59 | −2.511 87 | 0.389 92 | 1.826 98 | 1.797 45 |

by the width of $P_{Cu}(f_1,q)$. The most reasonable conjecture is that $P_{Cu}(f_1,q)$ has a structure due to the differences in the occupation of the second, third, and succeeding nearest-neighbor shells that can be described by the fractions $f_2$, $f_3$, etc. It would be interesting to obtain $P_{Cu}(f_1,q)$ to enough precision to see this effect, and also to calculate $P_{Cu}(f_1,f_2,q)$, $P_{Cu}(f_1,f_2,f_3,q)$, etc. Even with all of the computer time expended so far, there are still not enough charges to provide reliable statistics for that purpose, but the effect can be seen more easily by considering $P_{Cu}(q)$ for bcc disordered alloys calculated with the data published in Refs. 8 and 12 and discussed in Sec. IV C.

The function $P_{Cu}(q)$ shown in Fig. 18 represents the probability for a Cu atom in a bcc Cu-Zn alloy to have a charge between $q$ and $q+0.005$ electron charges, and was calculated by lumping together the charges for the five concentrations ranging from 10% to 90%. The function is certainly irregular, but it is difficult to count precisely the nine peaks that would correspond to the integer values of $n_{Zn}$ from zero to the number of atoms in the nearest-neighbor shell. The conditional probability $P_{Cu}(f_1,q)$ is also shown in Fig. 18 for $f_1=1/2$, and, as with the fcc alloys, knowledge of the fraction $f_1$ will improve the prediction of the charge on a given Cu atom. It appears that there are seven peaks in $P_{Cu}(f_1,q)$, which correspond to the possible occupations of the second-nearest-neighbor shell in the bcc structure. It is easy to imagine $P_{Cu}(f_1,q)$ as being the superposition of seven conditional probabilities $P_{Cu}(f_1,f_2,q)$ that would correspond to specific occupations of the first- and second-nearest-neighbor shells, but it can be seen from Fig. 18 that the $P_{Cu}(f_1,f_2,q)$ would also have finite widths due to the effects of still more distant neighbors.

The calculations shown here are certainly accurate enough to prove that the conditional probabilities, $P_{Cu}(f_1,q)$ and $P_{Cu}(f_1,f_2,q)$, have finite widths. With the interpretation of the origin of these widths and also with the numerical demonstrations in Sec. III of the long-range nature of the Coulomb interaction in alloys, it is difficult to arrive at any conclusion other than that the conditional probabilities $P_{Cu}(f_1,f_2,\ldots,q)$ will have a finite width when the fractional occupations of any finite number of nn shells is specified in the infinite ideal alloy.

Another piece of evidence for the continuous distribution of charges in disordered alloys is the $qV$ relation illustrated in Figs. 1, 3, and 6. This relation indicates very subtle and long-range correlations between all the charges in the crystal, and is intrinsically incompatible with any discrete distribution of charges.

## V. COMPARISONS WITH OTHER THEORIES

Many of the recent studies of Coulomb energies in alloys refer to a model that was first proposed by Magri, Wei, and

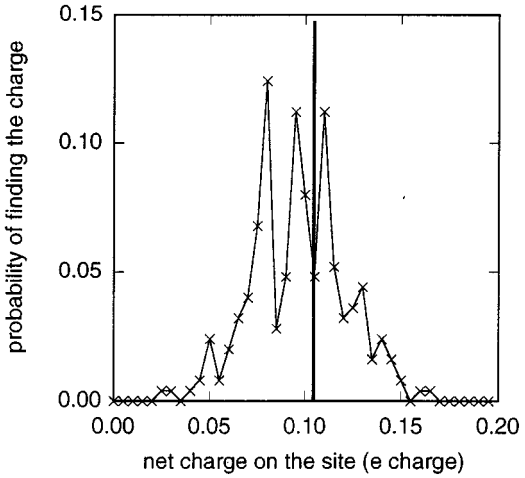


FIG. 16. The solid line with the points marked with crosses shows $P_{Cu}(c,q)$, the probability that a Cu atom in a fcc Cu-Zn alloy with a concentration $c=0.50$ will have a charge between $q$ and $q+0.005$ electron charges. The vertical line shows the average charge for the Cu atoms.

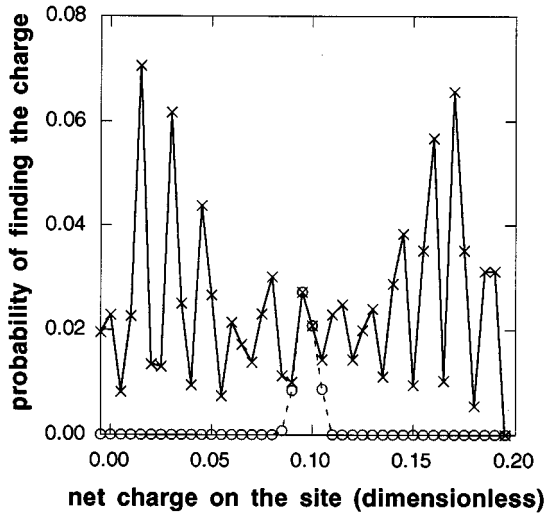


FIG. 17. The solid line with the points marked with crosses shows $P_{Cu}(q)$, the probability that a Cu atom in a fcc Cu-Zn alloy will have a charge between $q$ and $q+0.005$ electron charges. The circles connected with dashed lines shows the conditional probability $P_{Cu}(f_1,q)$, which is the probability that a Cu atom in a fcc Cu-Zn alloy that has a fraction $f_1$ of Cu atoms on the nearest-neighbor shell will have a charge between $q$ and $q+0.005$ electron charges. The data shown are for $f_1=1/2$.

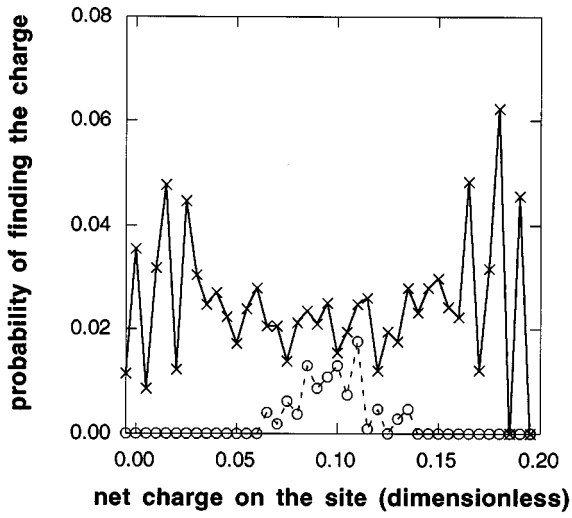


FIG. 18. The solid line with the points marked with crosses shows $P_{\mathrm{Cu}}(q)$, the probability that a Cu atom in a bcc Cu-Zn alloy will have a charge between $q$ and $q+0.005$ electron charges. The circles connected with dashed lines shows the conditional probability $P_{\mathrm{Cu}}(c_1,q)$, which is the probability that a Cu atom in a bcc Cu-Zn alloy that has a fraction $f_1$ of Cu atoms on the nearest-neighbor shell will have a charge between $q$ and $q+0.005$ electron charges. The data shown are for $f_1=1/2$.

Zunger (MWZ) in Ref. 1. In the MWZ model, the charge on a site containing a copper or zinc atom is given by

$$q^i=2\lambda n_{\mathrm{Zn}};\quad i\subset\mathrm{Cu},\quad q^i=-2\lambda n_{\mathrm{Cu}};\quad i\subset\mathrm{Zn}, \tag{46}$$

where $n_{\mathrm{Zn}}$ and $n_{\mathrm{Cu}}$ are the number of zinc or copper atoms in the first-nearest-neighbor shell. It is further assumed that $\lambda$ is independent of the concentration of the alloy, and that it can be calculated from the charges in ordered compounds containing a relatively small number of atoms in a unit cell. This is equivalent to the assumption that the conditional probability functions defined in the previous section, $P_{\mathrm{Cu}}(f_1,q)$ and $P_{\mathrm{Zn}}(f_1,q)$, are $\delta$ functions. This assumption is not consistent with extrapolations from our calculations. In principle, none of the conditional probabilities, $P_{\mathrm{Cu}}(f_1,q)$, $P_{\mathrm{Cu}}(f_1,f_2,q)$, etc., can be replaced by $\delta$ functions, although it may be a useful approximation in certain circumstances.

In the MWZ model, the average charge on the Cu site is $\langle q\rangle_{\mathrm{Cu}}=2\lambda W_1(1-c)$ with $\langle q\rangle_{\mathrm{Zn}}=-2\lambda W_1 c$ on the Zn site, where $W_1$ is the number of atoms in the first-nearest-neighbor shell. It follows that the difference between $\langle q\rangle_{\mathrm{Cu}}$ and $\langle q\rangle_{\mathrm{Zn}}$, $\Delta$, is independent of concentration in this model

$$\Delta=2\lambda W_1. \tag{47}$$

The difference $\Delta$ is plotted in Fig. 9 as a function of the concentration for the fcc and bcc Cu-Zn alloys and the fcc Cu-Pd alloys. It is very nearly constant for the Cu-Zn alloys, but it changes quite a bit with concentration for the Cu-Pd alloys.

The relations in Eq. (46) combined with a rule for the spatial distribution of the atoms in the crystal determines all the charge-charge correlation functions for the crystal. For ideally random alloys, the MWZ model leads to the correlations

$$\langle q(0)q(\mathbf{a}_k)\rangle=4\lambda^2c(1-c)[W_1^2+W_1],\quad \mathbf{a}_k=0,$$

$$\langle q(0)q(\mathbf{a}_k)\rangle=4\lambda^2c(1-c)[-2W_1+K_1],\quad \mathbf{a}_k=r_1,$$

$$\langle q(0)q(\mathbf{a}_k)\rangle=4\lambda^2c(1-c)K_n,\quad \mathbf{a}_k=r_n,\ n>1, \tag{48}$$

where $r_n$ is the radius of the $n$th nearest-neighbor shell and $K_n$ is the number of atoms that are common to nearest-neighbor shells centered on the central atom and on an atom of the $n$th nearest-neighbor shell. These parameters have been discussed more fully in Ref. 2. The sum rule in Eq. (35) is satisfied by these correlation functions as a consequence of the relation

$$\sum_{n=1}^{\infty} W_nK_n=W_1{}^2-W_1, \tag{49}$$

where $W_n$ is the number of atoms in the $n$th nearest-neighbor shell. For fcc crystals, $K_n$ is zero for $n>4$, while for bcc crystals $K_n$ is zero for $n>5$. These are very specific predictions for the correlation functions, and they lead to equally specific predictions about the interatomic Coulomb energy $u_C^q$.

Writing $\mathbf{a}_j$ in Eq. (20) as $\mathbf{a}_j=\mathbf{a}_i+\mathbf{a}_k$ and carrying out the summations leads to the following form for $U_C^q$:

$$U_C^q=\sum_{k=1}^{N}{}' \sum_p \frac{\langle q(0)q(\mathbf{a}_k)\rangle}{|\mathbf{a}_k+\mathbf{R}_p|}, \tag{50}$$

where in this case the prime means that $a_k\neq 0$. Inserting the correlation functions of Eq. (35) into the expression in Eq. (50) leads to a formula for the interatomic Coulomb energy from the MWZ model that can be split into two parts in a fashion that is analogous to Eq. (31),

$$u_C^{\mathrm{MWZ}}=u_1^{\mathrm{MWZ}}+u_2^{\mathrm{MWZ}}. \tag{51}$$

The approximation to $u_{C1}$ may be written

$$u_1^{\mathrm{MWZ}}=-\frac{\Delta^2}{r_1}\,c(1-c), \tag{52}$$

with $\Delta$ given by Eq. (33), and the approximation to $u_{C2}$ is

$$u_2^{\mathrm{MWZ}}=u_1^{\mathrm{MWZ}}\left(1-\frac{1}{W_1{}^2}\sum_n \frac{r_1}{r_n}\,W_nK_n\right). \tag{53}$$

This formula is algebraically identical with the one described in Ref. 2, although its derivation and interpretation are somewhat different. Interatomic Coulomb energies derived from these same assumptions have been used in an extensive study of the short- and long-range order in models of binary alloys in which this is the only interaction, see Ref. 6. For a suitable value of $\lambda$, the predictions of the MWZ model for $u_C^q$ will be qualitatively correct, but it is useful to understand the features of these predictions that are representative of real alloys and those that are peculiarities of the model.

Using Eqs. (28) and (33) it can be shown that the expression for $u_{C1}$ in Eq. (32) is equivalent to

$$u_{C1}=\tfrac{1}{2}\alpha\Delta^2c(1-c). \tag{54}$$

Comparing this with Eq. (52) it is seen that $u_1^{\mathrm{MWZ}}$ would be the same as $u_{C1}$ if it is assumed that the difference in the

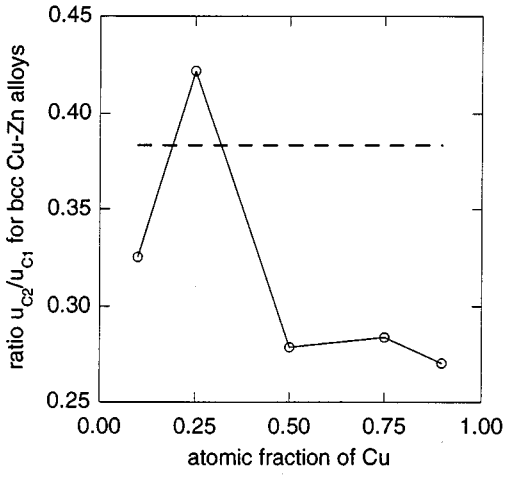


FIG. 19. Ratios of the two contributions to the Coulomb energy $u_{C1}/u_{C2}$ for bcc Cu-Zn alloys calculated with 432 atoms in the cell. The dashed line is the prediction of the MWZ model.

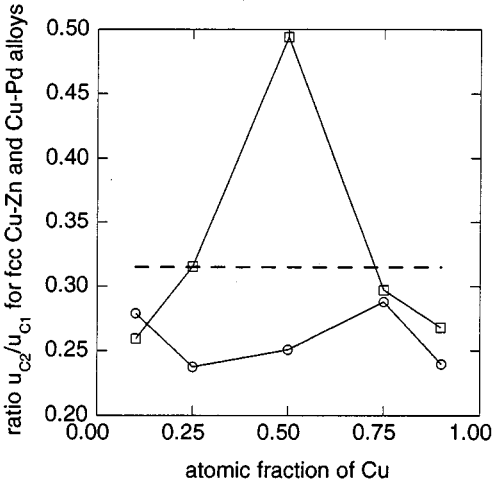


FIG. 20. Ratios of the two contributions to the Coulomb energy $u_{C1}/u_{C2}$ for fcc alloys. The circles are the values for Cu-Zn alloys calculated with 500 atoms in the cell, and the squares are for Cu-Pd alloys calculated with 256 atoms in the cell. The dashed line is the prediction of the MWZ model.

average charges of the two atoms, $\Delta$, is independent of concentration and that $\alpha$ is exactly $2/r_1$. It predicts that $u_{C1}$ is precisely a parabolic function of $c$ with its minimum at $c=0.5$. As expected from the variation of $\Delta$ with $c$ illustrated in Fig. 9 and the variation of $\alpha$ with $c$ from Figs. 10 and 11, $u_{C1}$ is slightly asymmetric for the Cu-Zn alloys shown in Fig. 5 and quite asymmetric for the Cu-Pd alloys shown in Fig. 8.

The second term, $u_2^{\mathrm{MWZ}}$, is different in magnitude and in physical origin from the $u_{C2}$ in Eq. (32). This is illustrated graphically by the prediction of the MWZ model that the ratio of the energies $u_{C2}/u_{C1}$ is a constant that is independent of the concentration of the alloy. An even more striking aspect of this prediction is that the ratio is independent of the constituents of the alloy. The ratio $u_2^{\mathrm{MWZ}}/u_1^{\mathrm{MWZ}}$ is the quantity in the parentheses in Eq. (53), and it is 0.383 13 for all random alloys that have the bcc structure and 0.314 72 for all those with the fcc structure. The ratios $u_{C2}/u_{C1}$ from the LDA calculations for the bcc Cu-Zn alloys are plotted against the concentration in Fig. 19, and it is obvious that they change a great deal with concentration. As for the ratio being independent of the alloy constituents, $u_{C2}/u_{C1}$ is plotted in Fig. 20 for the fcc Cu-Zn and Cu-Pd alloys, and it can be seen that they are quite different.

Very recently, a paper has been published[37] that revisits the MWZ model in light of the LSMS calculations in Refs. 7 and 12 that we published earlier. They show a calculation of the $qV$ relation that would be obtained for our alloy models that are modified by replacing the actual charges on the sites by the charges that would be predicted to be on the sites by Eq. (46), the value of $\lambda$ being taken from a fit to the center of the peaks in the conditional probabilities $P_{\mathrm{Cu}}(f_1,q)$ and $P_{\mathrm{Zn}}(f_1,q)$. These results, shown in their Fig. 2, illustrate the point made above that our $qV$ relation is fundamentally incompatible with a model that predicts that the charges on lattice sites can take on only a small number of values. In the MWZ model there are only nine possible charges on a copper or zinc site in a bcc alloy, and twelve in fcc. They also derive a formula from the MWZ model that relates the average potential for a given charge to that charge, and show that this would be a straight line. This is not the $qV$ relation we are discussing. Their prediction for the slopes $\gamma_{\mathrm{Cu}}$ and $\gamma_{\mathrm{Zn}}$ are quantitatively not very accurate. More importantly, they predict that $\gamma_{\mathrm{Cu}}=\gamma_{\mathrm{Zn}}$ and the slopes should be independent of concentration. It can be seen from Fig. 12 that this is not the case.

Another aspect of this paper that is relevant to the present discussion is that they propose to replace the MWZ model with a model in which the numbers of atoms in the nearest-neighbor shells $n_{\mathrm{Cu}}$ and $n_{\mathrm{Zn}}$ in Eq. (46) are replaced with effective numbers that include constants $x_2$, $x_3$,..., times the number of copper or zinc atoms in the second, third, etc., nearest-neighbor shells. Of course, one now must fit to the results of a reliable LDA calculation of the LSMS type to find not only the $\lambda$ but also the constants that multiply the numbers of atoms in the more distant shells. The numbers that they publish for fcc copper-zinc alloys will not work, for example, for fcc copper-palladium alloys. However, as more nearest-neighbor shells are taken into account, the differences between the picture presented by this model becomes less different from the one described in this paper. The number of possible charges increases from 12 to 72 to 1728 for fcc and from 8 to 48 to 576 for bcc as the number of nearest-neighbor shells increases from one to two to three. This is rapidly approaching the infinity of possible charges that we believe should be assumed. In addition, the number of nearest-neighbor shells in their model is approaching the number that we have in our local interaction zones, which is four for fcc and five for bcc. Of course, we include the Coulomb interactions with an infinity of atoms.

The theories for the interatomic Coulomb energy described in Refs. 3–5 are based on the coherent-potential approximation (CPA),[38] which is an excellent theory for the electronic states of substitutional disordered alloys when good potential functions for the constituents of the alloy are provided. The CPA does not contain a prescription for calculating charge self-consistent potentials, and the method used until recently[39] assumes that the Coulomb potentials at the sites $V^i$ are zero. In its usual form, the CPA provides the average charges, e.g., $\langle q\rangle_{\mathrm{Cu}}$ and $\langle q\rangle_{\mathrm{Zn}}$, but no information

about the fluctuations of charge about this average. The modified CPA theories (MCPA) of Refs. 3–5 are based on the assumption that $\langle q\rangle_{\mathrm{Cu}}$ and $\langle q\rangle_{\mathrm{Zn}}$ can be found by assuming the average Coulomb shifts $\langle V(n)\rangle_{\mathrm{Cu}}$ and $\langle V(n)\rangle_{\mathrm{Zn}}$ are zero for $n>1$. This is roughly correct, as can be seen from Fig. 2. The value for $\alpha$ that comes from the screening assumption of the MCPA is $2.0/r_1$, which we have shown in Figs. 10 and 11 is reliable to within about 10%. It is thus possible that one can calculate improved values of $\langle q\rangle_{\mathrm{Cu}}$ and $\langle q\rangle_{\mathrm{Zn}}$ from the MCPA, although it cannot predict the actual charge on any particular site in a real alloy as explained in Sec. IV A. The energy $u_{C1}$ is written in terms of $\langle q\rangle_{\mathrm{Cu}}$ and $\langle q\rangle_{\mathrm{Zn}}$ in Eq. (32), and it can be calculated from any version of the CPA. The CPA results are not as restricted as the ones from the MWZ model because there is no assumption that $\Delta$ is independent of concentration.

The fact that the MCPA gives $u_{C1}$ but not $u_{C2}$ was recognized, and a proposal was made in Ref. 5 to use the Connolly-Williams (CW) method[40] to estimate the corrections. In the CW method, information about the electronic structure for ordered intermetallic compounds containing a relatively small number of atoms in a unit cell is used to estimate the properties of the disordered alloy. This approach had only limited success.

Some of these same authors have made another proposal that appears more promising, and have used it in calculations on Cu-Zn alloys.[41] They combined the idea of the LSMS with the CPA to develop a charge self-consistent CPA that, among other advantages, includes $u_{C2}$ automatically. A later application of this locally self-consistent Green's-function method (LSGF) to Pd-Rh alloys provides more evidence that it is a useful approach.[42] The LSGF goes beyond the older CPA's in that it correctly takes into account the fact that every atom has a different charge, and it treats the Coulomb energy as accurately as the LSMS. It still contains the essential feature of the CPA in that it leads to a Green's function for the disordered alloy that has the same form as the Green's function for a periodic solid, but with a very complicated effective scatterer on each site.

In the pioneering work on alloy theory by Mott,[43] Friedel,[44] Gautier, DuCastelle,[45] and Pettifor,[46] the interatomic Coulomb energy is simply ignored, and this is also true of much of the work done using the CPA.[47] The results shown in Fig. 5 can be used as a justification for that position. Not only are the Coulomb energies for the copper-zinc alloys small, but they are remarkably insensitive to the crystal structure. They are larger for Cu-Pd alloys, but are probably still not very dependent on structure for the relatively small number of crystal structures that one encounters in metallic alloys.

## VI. DISCUSSION

In Ref. 12, an analysis of the fundamental DFT-LDA equations was used to argue for the occurrence of the $qV$ relation. It was pointed out that a consequence of this relation is the expression for $U_C^q$ in Eq. (32) that is local in the sense that it can be written as a sum of single-site terms. As far as can be seen, this expression is exact if the charges come from a self-consistent DFT-LDA calculation. An implication of this result is that, if one has the five basic parameters $\alpha$, $\langle q\rangle_{\mathrm{Cu}}$, $\langle q\rangle_{\mathrm{Zn}}$, $\beta_{\mathrm{Cu}}$, and $\beta_{\mathrm{Zn}}$, the contribution that a given charge on a site $q^i$ makes to $U_C^q$ is known, without any specific information about the other charges in the system. This is really a surprising and counter-intuitive result. It can have practical applications, because there are useful approximate methods, such as the embedded-cluster method,[48] that provide exactly that information.

At the present time, an order-$N$ calculation like the one described here seems to be the only reliable method for obtaining the interatomic Coulomb energy for a disordered alloy, or for obtaining the five basic parameters listed above. This is not as bad as it sounds, because a relatively small calculation, $N=256$, should be adequate. With a massively parallel supercomputer and a well-developed program, that calculation is not difficult. Potentials obtained by a straightforward averaging of the self-consistent atomic potentials obtained in the LSMS calculations have been used in CPA calculations. The average charges on the sites obtained from this CPA calculation are identical to the average charges from the LSMS. There is no trivial explanation for this result, and it indicates that the theories are not incompatible. Another possible way of approaching these calculations is the LSGF-CPA method of Abrikosov *et al.* in Ref. 41. One could imagine using the LSMS for the things that it does best and the CPA for the things that it does best, such as investigating Fermi-surface effects in alloys.

The connection between the slope $\alpha$ and the nearest-neighbor radius and the relations between the $\beta_{\mathrm{Cu}}$ and $\beta_{\mathrm{Zn}}$ with the average densities of states at the Fermi energy, which were pointed out in Sec. IV, are interesting, but they do not constitute a theory. It is to be hoped that the insights into this problem that have been gained from the LSMS calculations can be used to develop a more analytical approach to the Coulomb energies, and indeed other aspects of alloy theory. This would not only make it possible to obtain the desired results with less computation, but would give more physical insight into the results.

Finally, the argument based on experimental evidence that atomic size effects will not affect the results of the calculations described in this paper appreciably, given in Sec. II B, should not be construed to indicate that the authors consider size effects to be uninteresting. One of our goals is to use the LSMS in Car-Parinello[49] type calculations to study the effect of atomic size on the total energies of metallic alloys.

## ACKNOWLEDGMENTS

This work was supported by the U.S. Department of Energy, Division of Materials Science, Office of Basic Energy Sciences under Subcontract No. DE-ACO5-84OR21400 with Martin Marietta Energy Systems, Inc., and by the Federal High Performance Computing and Communications program, Applied Mathematical Sciences Program, Office of Energy Research. We made use of the Intel Paragon XP/S-150 massively parallel supercomputer at the Oak Ridge National Laboratory.

[1] R. Magri, S. H. Wei, and A. Zunger, Phys. Rev. B **42**, 11 388 (1990).
[2] Z. W. Lu, S.-H. Wei, A. Zunger, S. Frota-Pessoa, and L. G. Ferreira, Phys. Rev. B **44**, 512 (1991).
[3] I. A. Abrikosov, Yu. H. Vekilov, P. A. Korzhavyi, A. V. Ruban, and L. E. Shilkrot, Solid State Commun. **83**, 867 (1992).
[4] D. D. Johnson and F. J. Pinski, Phys. Rev. B **48**, 11 553 (1993).
[5] P. A. Korzhavyi, A. V. Ruban, I. A. Abrikosov, and H. L. Skriver, Phys. Rev. B **51**, 5773 (1995).
[6] C. Wolverton and A. Zunger, Phys. Rev. B **51**, 6876 (1995).
[7] J. S. Faulkner, Yang Wang, and G. M. Stocks, in *Alloy Modeling and Design*, edited by G. M. Stocks, C. T. Liu, and P. E. A. Turchi (The Minerals, Metals, and Materials Society, Warrendale, PA, 1995).
[8] J. S. Faulkner, Yang Wang, and G. M. Stocks, in the *Proceedings of the NATO-ASI Stability of Materials*, Vol. 355 of *NATO Advanced Study Institute*, Series B: Physics, edited by A. Gonis, P. E. A. Turchi, and J. Kudrnovsky (Plenum, New York, 1996).
[9] I. A. Abrikosov, A. V. Ruban, B. Johansson, and H. L. Skriver, in the *Proceedings of the NATO-ASI Stability of Materials*, Vol. XX of *NATO Advanced Study Institute*, Series E: Applied Sciences, edited by A. Gonis, P. E. A. Turchi, and J. Kudrnovsky (Kluwer, the Netherlands, 1996).
[10] W. Kohn and L. J. Sham, Phys. Rev. **140**, A1133 (1965).
[11] Y. Wang, G. M. Stocks, W. A. Shelton, D. M. C. Nicholson, Z. Szotek, and W. M. Temmermann, Phys. Rev. Lett. **75**, 2867 (1995).
[12] J. S. Faulkner, Yang Wang, and G. M. Stocks, Phys. Rev. B **52**, 17 106 (1995).
[13] William Hume-Rothery, R. E. Smallman, and C. W. Haworth, *The Structure of Metals and Alloys* (The Institute of Metals, London, 1969).
[14] Hohenberg and W. Kohn, Phys. Rev. **136**, B864 (1964).
[15] P. P. Ewald, Ann. Phys. (Leipzig) **64**, 253 (1921).
[16] S. Asano and J. Yamashita, J. Phys. Soc. Jpn. **30**, 667 (1971).
[17] S. G. Louie, K. Ho, and M. L. Cohen, Phys. Rev. B **19**, 1774 (1979); J. Neve, B. Sundqvist, and O. Rapp, *ibid.* **28**, 629 (1983); A. R. Jani, N. E. Brenner, and J. Callaway, *ibid.* **38**, 9425 (1988); D. M. Nicholson and J. S. Faulkner, *ibid.* **39**, 8187 (1989).
[18] *Theory of X-Ray and Thermal-Neutron Scattering*, edited by M. A. Krivoglaz (Plenum, New York, 1969).
[19] D. I. Vadets, V. A. Val'chikovskaya, S. E. Naminskaya, and Yu. I. Perel', Sov. Phys. J. **16**, 1769 (1973).
[20] F. H. Herbstein, B. S. Borie, Jr., and B. L. Averbach, Acta Crystallogr. **9**, 466 (1956).
[21] X. Jiang, G. E. Ice, C. J. Sparks, L. Robertson, and P. Zschack, Phys. Rev. B **54**, 3211 (1996).
[22] A more detailed discussion of the sense in which these samples can be considered to be random is given in Sec. IV.
[23] G. M. Stocks, D. M. C. Nicholson, Y. Wang, W. A. Shelton, Z. Szotek, and W. M. Temmermann, in *High Performance Computing Symposium; Grand Challenges in Computer Simulation*, Proceedings of the 1994 Simulation Multiconference, edited by A. M. Tentner (The Society for Computer Simulation, San Diego, CA, 1994); D. M. C. Nicholson, G. M. Stocks, Y. Wang, W. A. Shelton, Z. Szotek, and W. M. Temmermann, Phys. Rev. B **50**, 14 686 (1994).
[24] Yang Wang, G. M. Stocks, W. A. Shelton, D. M. C. Nicholson, Z. Szotek, and W. M. Temmerman, Phys. Rev. Lett. **75**, 2867 (1995).
[25] Lord Rayleigh, Philos. Mag. **34**, 481 (1892).
[26] J. Korringa, Physica **13**, 392 (1947); W. Kohn and N. Rostoker, Phys. Rev. **94**, 111 (1954).
[27] W. Kohn, Phys. Rev. Lett. **76**, 3168 (1996).
[28] J. Harris, Phys. Rev. B **31**, 1770 (1985).
[29] J. M. Cowley, J. Appl. Phys. **21**, 24 (1950).
[30] P. W. Anderson, Science **177**, 393 (1972).
[31] P. W. Anderson, Phys. Rev. **109**, 1492 (1958).
[32] H. Yang, J. C. Swihart, D. M. C. Nicholson, and R. H. Brown, Phys. Rev. B **47**, 107 (1993); D. M. C. Nicholson and R. H. Brown, Phys. Rev. Lett. **70**, 3311 (1993).
[33] I. M. Lifschitz, Sov. Phys. JETP **17**, 1159 (1963).
[34] J. S. Faulkner, Prog. Mater. Sci. **27**, 1 (1982).
[35] R. Alben, M. Blume, and M. Mckeown, Phys. Rev. B **16**, 3829 (1977).
[36] C. B. Walker and D. T. Keating, Phys. Rev. **130**, 1726 (1963); L. Reinhard, B. Schonfeld, G. Kostorz, and W. Buhrer, Phys. Rev. B **41**, 1727 (1990).
[37] C. Wolverton, A. Zunger, S. Froyen, and S.-H. Wei, Phys. Rev. B **54**, 7843 (1996).
[38] P. Soven, Phys. Rev. **156**, 809 (1967); **178**, 1136 (1969).
[39] H. Winter and G. M. Stocks, Phys. Rev. B **27**, 882 (1983).
[40] J. W. D. Conolly and A. R. Williams, Phys. Rev. B **27**, 5169 (1983).
[41] I. A. Abrikosov, A. M. N. Niklasson, S. I. Simak, B. Johansson, A. V. Ruban, and H. L. Skriver, Phys. Rev. Lett. **76**, 4203 (1996).
[42] I. A. Abrikosov, S. I. Simak, and B. Johansson, in *The Proceedings of the First International Alloy Conference (IAC-1)*, edited by A. Gonis, A. Meike, and P. E. A. Turchi (Plenum, New York, 1996).
[43] N. F. Mott and H. Jones, *The Theory of the Properties of Metals and Alloys* (Dover, New York, 1958).
[44] J. Friedel, in *The Physics of Metals*, edited by J. M. Ziman (Cambridge University Press, Cambridge, U.K., 1969), Chap. 8.
[45] F. Ducastelle, *Order and Phase Stability in Alloys* (North-Holland, Amsterdam, 1991).
[46] D. G. Pettifor, in *Physical Metallurgy*, edited by R. W. Cahn and P. Haasen (Elsevier, Holland, 1983).
[47] B. L. Gyorffy, D. D. Johnson, F. J. Pinski, D. M. Nicholson, and G. M. Stocks, in *Alloy Phase Stability*, edited by G. M. Stocks and A. Gonis, Vol. 163 of *NATO Advanced Study Institute, Series E: Applied Sciences* (Kluwer, The Netherlands, 1989).
[48] A. Gonis, W. H. Butler, and G. M. Stocks, Phys. Rev. Lett. **50**, 1482 (1983); A. Gonis, G. M. Stocks, W. H. Butler, and H. Winter, Phys. Rev. B **29**, 555 (1984).
[49] R. Car and M. Parrinello, Phys. Rev. Lett. **55**, 2471 (1985).